Identification of Histidine 105 in the β1 Subunit of Soluble Guanylate Cyclase as the Heme Proximal Ligand†

Yunde Zhao,‡ Johannes P. M. Schelvis,§ Gerald T. Babcock,*,§ and Michael A. Marletta*,‡,||,⊥

Department of Biological Chemistry, School of Medicine, Howard Hughes Medical Institute, and Interdepartmental Program in Medicinal Chemistry, College of Pharmacy, The University of Michigan, Ann Arbor, Michigan 48109-1065, and Department of Chemistry and the LASER Laboratory, Michigan State University, East Lansing, Michigan 48824-1322.

Received October 29, 1997; Revised Manuscript Received February 3, 1998

ABSTRACT: Soluble guanylate cyclase isolated from bovine and rat lung is a heterodimeric hemoprotein composed of α1 and β1 subunits. The heme binding region has been localized to residues 1−385 of the β1 subunit [β1(1−385)], while the catalytic site(s) have been localized to the C-terminal region of sGC. There are four conserved histidine residues in the heme binding region of sGC. H220 and H346 are conserved among all known sGC subunits (α and β), while H105 and H134 are conserved only in the β subunits (β1 and β2). Site-directed mutagenesis was used to individually change each of the conserved histidines in sGC β1(1−385) to alanine or glycine, and the resulting mutants were expressed in *E. coli*. All of the mutants except for H105A and H105G had heme bound as isolated. Imidazole (Im) was able to rescue heme binding to H105G when added to the growth medium and purification buffers. The heme in H105G isolated in the presence of imidazole [H105G(Im)] was ferric and a mixture of 5-coordinate, high-spin and 6-coordinate, low-spin complexes. After reduction, the ferrous heme in H105G(Im) was 5-coordinate, high-spin as indicated by resonance Raman spectroscopy. When imidazole in H105G(Im) was exchanged with *N*-methylimidazole (MeIm), the Fe−N(Im/MeIm) stretching frequency was shifted from 221 to 212 cm^{-1}. A shift of this magnitude is expected when the ligand is directly coordinated to the heme iron. All of the data are consistent with the conclusion that H105 in the β1 subunit is the heme proximal ligand.

Guanylate cyclase (EC 4.6.1.2) catalyzes the conversion of GTP[1] to cGMP and pyrophosphate (*1, 2*). Two general types of guanylate cyclases have been characterized: particulate guanylate cyclases (pGC) and soluble guanylate cyclases (sGC). pGC activity is regulated by small peptide hormones such as A-type natriuretic peptide and B-type natriuretic peptide; sGC activity is regulated by nitric oxide (NO) (*1, 3, 4*). NO, a signaling molecule involved in several biological processes including vasodilation and neuronal signaling (*5*−*7*), has been shown to activate sGC up to 400-fold over its basal activity. To date, sGC is the only known receptor for NO. sGC purified from mammalian lung tissue is a heterodimeric hemoprotein composed of α1 and β1 subunits (*8*−*12*). To date, four different isoforms of sGC (α1, α2, β1, and β2) have been identified at the cDNA level (*13, 14*), but only α1 and β1 subunits have been characterized at the protein level. The formation of an α1β1 heterodimer appears to be necessary for sGC activity because transfection of COS cells with cDNAs encoding either α1 or β1 subunits alone did not produce active enzyme. Only coexpression of the α1 and β1 subunits of sGC produced active enzyme (*15, 16*). All sGC subunits have a homologous C-terminal region that is also homologous to the catalytic domain of pGC and adenylate cyclase (*1*). When the C-terminal regions of sGC [α1(367−691) and β1(306−619)] were coexpressed in COS cells, basal sGC activity but not NO-stimulated activity was detected (*17, 18*). The C-terminal region of sGC, therefore, has been assigned as the catalytic site(s), although it is not known whether there is one active site in each subunit (α1 and β1) or whether the active site is formed using residues from both subunits. The N-terminal region of sGC is not homologous to any other known protein. Recently, we have localized the heme binding region of sGC to the N-terminal 385 amino acid residues of the β1 subunit. Expressed in *E. coli* and purified to homogeneity, β1(1−385) itself is sufficient for heme binding (*19*).

Activation of sGC by NO results from the interaction of NO with the heme of sGC. Spectroscopic studies have shown that the heme in sGC is ferrous, high-spin, and 5-coordinate with a histidine residue as the only axial ligand (*12, 20, 21*). Binding of NO to the heme in sGC results in the formation of a 5-coordinate nitrosyl complex by severing

† The studies were supported by a Searle chair endowment fund, by the Howard Hughes Medical Institute, and by NIH Grant GM25480.

* To whom correspondence should be addressed.

‡ Department of Biological Chemistry, The University of Michigan.

§ Department of Chemistry and the LASER Laboratory, Michigan State University.

|| Howard Hughes Medical Institute, The University of Michigan.

⊥ Interdepartmental Program in Medicinal Chemistry, The University of Michigan.

[1] Abbreviations: apoH105G, H105G mutant without bound heme; BSA, bovine serum albumin; cGMP, guanosine 3′,5′-cyclic monophosphate; DTT, dithiothreitol; GTP, guanosine 5′-triphosphate; H105G(Im), H105G mutant expressed and purified in the presence of imidazole with heme bound; Im, imidazole; IPTG, isopropyl β-D-thiogalactopyranoside; MeIm, *N*-methylimidazole; pGC, particulate guanylate cyclase; PCR, polymerase chain reaction; sGC, soluble guanylate cyclase; wt, wild type.

S0006-2960(97)02686-X CCC: $15.00
Published on Web 03/12/1998

the bond between the proximal amino acid ligand and the heme iron (*22*, *23*), whereas the nitrosyl complex of myoglobin is 6-coordinate (*24*). Formation of a 5-coordinate nitrosyl complex in sGC, in contrast to myoglobin, may be due to the weak histidine−iron bond in sGC as demonstrated by resonance Raman spectroscopy (*20*, *25*). Identification of the heme proximal ligand of sGC and characterization of the heme environment will help elucidate both the interaction between NO and sGC and the mechanism of NO activation. In this study, site-directed mutagenesis, electronic absorption spectroscopy, and resonance Raman spectroscopy were employed to identify H105 in the β1 subunit as the heme proximal ligand of sGC.

MATERIALS AND METHODS

Materials. Rat lung sGC cDNAs were kindly provided by Dr. Masaki Nakane of Abbott Laboratories. The plasmid pET-20b and *E. coli* BL21(DE3)pLysS competent cells were purchased from Novagen. The Expand High Fidelity PCR kit was obtained from Boehringer Mannheim. Restriction enzymes, T4 DNA ligase, and IPTG were purchased from Gibco BRL. The plasmid purification kit and gel extraction kit for recovering DNA from agarose gels were purchased from Qiagen. TSK DEAE 650M anion-exchange resin was purchased from TosoHaas. The Superdex 200 HiLoad 26/60 gel filtration column was from Pharmacia. Bradford protein dye reagent was purchased from Bio-Rad. Carbon monoxide (99.5%) and nitric oxide (99.0%) were from Matheson. Site-directed mutagenesis primers were synthesized by the Biomedical Research Core Facility, The University of Michigan. All other chemicals were purchased from Sigma Chemical Co. unless otherwise stated.

Site-Directed Mutagenesis. Site-directed mutagenesis of the conserved histidines was carried out using the DNA polymerase chain reaction (PCR) method (*26*). The external primers for H105A, H105G, and H134A mutants were 5′-CATATGTACGGTTTTGTGAACCAT-3′ and 5′-CTGGGTACCGTTCTCTTCGAACCTGTCCAGATC-3′. The mutagenic primers for H105A were 5′-CCTCGACGCCCTGGCCGACCACCTCGCCAC-3′ and 5′-GTGGCGAGGTGGTCGGCCAGGGCGTCGAGG-3′. The mutagenic primers for H105G were 5′-GTGGCGAGGTGGTCTCCCAGGGCGTCGAGG-3′ and 5′-CCTCGACGCCCTGGGAGACCACCTCGCCAC-3′. The mutagenic primers for H134A were 5′-TCTTTCCGAGTAGTAGGCCAGAATGAGCCC-3′ and 5′-GGGCTCATTCTGGCCTACTACTCGGAAAGA-3′. The PCR fragments with mutations for H105A, H105G, and H134A were used to replace the corresponding wild-type (wt) fragment in β1(1−385) using restriction enzymes *Kpn*I/*Nde*I. The external primers for H220A and H346A were 5′-GAAGAGAACGGTACCCACCTC-3′ and 5′-GGATCCTAATCCTCCAAAGCCCTCAG-3′. The mutagenic primers for H220A were 5′-CCGGTCAAATATGATGGCAAAAGGAAACGC-3′ and 5′-GCGTTTCCTTTTGCCATCATATTTGACCGG-3′. The mutagenic primers for H346A were 5′-CTCGTGTAGCATCAGCGAGAGGGATGTACA-3′ and 5′-GTGACATCCCTCTCGCTGATGCTACACGAG-3′. The PCR fragments for H220A and H346A were used to replace the corresponding wt fragments in β1(1−385) using *Kpn*I/*Bam*HI. The fidelity of the PCR reactions and the mutations was confirmed by DNA sequencing.

Expression of wt and Mutant β1(1−385) in E. coli. wt β1(1−385) was expressed as described previously (*19*). H105A, apoH105G, H134A, H220A, and H346A mutants of β1(1−385) were expressed using the same conditions as for wt β1(1−385) except that the mutant cultures were harvested 10−12 h after IPTG induction as compared to 12−14 h for wt β1(1−385). The heme-containing H105G(Im) was expressed using the same conditions as those used for the other mutants except that 10 mM imidazole was included in the growth medium.

Purification of wt β1(1−385) and Related Mutants. wt β1(1−385), H134A, H220A, and H346A mutants were purified using a previously described method (*19*). ApoH105G and H105A were purified using a protocol similar to that used for wt β1(1−385); however, fractions containing apoH105G and H105A were identified by SDS−PAGE and Western blot analysis since they contained no Soret peak.

H105G(Im) was purified as follows: the frozen cell pellet from 3 L of culture was thawed on ice for about 2 h, resuspended in 120 mL of buffer A (50 mM Hepes, pH 7.4, 100 mM NaCl, 10 mM imidazole, and 1 mM PMSF), and lysed by sonication for 5 min on ice. The resulting homogenate was centrifuged at 100000*g* for 1 h. The supernatant from this centrifugation was applied to a TSK DEAE anion exchange column (2.5 cm × 25 cm) that had been equilibrated with buffer A. The DEAE column was washed with 300 mL of buffer A at a rate of 1.2 mL/min. H105G(Im) was eluted with a NaCl gradient from 100 mM to 500 mM in a total volume of 1 L. Fractions with $A_{280}/A_{\mathrm{Soret}}$ less than 1 were pooled and concentrated to 10 mL using an Amicon concentrator and a disk membrane (Filtron, 30 kDa MW cutoff). The concentrated sample was loaded onto a Superdex 200 HiLoad 26/60 gel filtration column equilibrated with buffer B (50 mM Hepes, pH 7.4, 150 mM NaCl, 10 mM imidazole). Fractions containing H105G(Im) were pooled and concentrated to the desired concentration.

Determination of Protein Concentration and Heme Content. Protein concentration was determined by the Bradford microassay using BSA as the standard. The Bradford assay was calibrated by quantitative amino acid analysis as previously described (*19*). Heme concentrations were determined by the pyridine−hemochromagen assay using horse heart myoglobin as the standard as previously described (*19*, *27*).

Estimation of the Native Molecular Weight of wt β1(1−385) and Related Mutants. The native molecular weight of wt β1(1−385) and mutants of this construct was estimated using gel filtration as described (*19*).

Electronic Absorption Spectroscopy. Electronic absorption spectra were recorded on a Cary 3E spectrophotometer equipped with a Neslab RTE-100 temperature controller set at 10 °C. The NO and CO complexes of β1(1−385) and the mutants were formed as described previously (*19*). KCN (250 mM) was added to H105G(Im) to form a cyano−heme complex. The bis(imidazole) complex of the heme containing H105G(Im) was formed by incubating H105G(Im) with 300 mM imidazole at 10 °C for 3 h.

Resonance Raman Spectroscopy. Samples of wt β1(1−385) (80 μM) used for resonance Raman spectroscopy were prepared in 50 mM Hepes, pH 7.4, 150 mM NaCl, and 5 mM DTT. The spectra of ferrous wt β1(1−385) were obtained with 431 nm excitation using a dye laser with

Table 1: Effects of Histidine to Alanine Mutations of sGC β1(1−385) on Heme Binding, Soret Peak Position (nm), and Dimerization

samples	Soret (nm) as isolated	+CO	+NO	heme content[b]	oligomerization
wt β1(1−385)	431	423	399	0.9	dimer
H346A β1(1−385)	426	423	399	0.8	monomer
H220A β1(1−385)	426	423	399	0.9	dimer
H134A β1(1−385)	431	nd[a]	nd	nd	nd
H105A β1(1−385)	no heme				dimer

[a] nd, not determined. [b] Heme content is expressed as the ratio of the amount of heme bound as determined by the pyridine−hemochromgen assay to protein concentration.

stilbene 420 as the dye pumped with an Ar^+ laser (Coherent Innova 200). The sample of H105G(Im) (50 μM) was in 50 mM Hepes, pH 7.4, 150 mM NaCl, and 1 mM imidazole. To exchange imidazole in H105G(Im) with *N*-methylimidazole, H105G(Im) was purified as described above except there was no imidazole in the gel filtration mobile phase. After gel filtration, H105G(Im) was concentrated to 50 μM, and *N*-methylimidazole was added to a final concentration of 1 mM. The spectra for H105G(Im) were obtained with excitation at 413 nm using a Kr^+ laser (Coherent K-90). All spectra were collected using a spinning cell. The laser power was kept at 5 mW or less at all the wavelengths used. The laser light was focused on the sample by a lens with a focal length of 50 mm. The resonance Raman scattering was detected with a spectrometer (Spex 1877 Triplemate) in combination with a liquid nitrogen cooled CCD detector (EG&G OMA 4, Model 1530-CUV-1024S). Accumulation time is indicated in the figure legends. The resonance Raman modes of the heme have been labeled according to the porphyrin mode numbering system introduced by Abe et al. (*28*). The mode assignments are based on the assignments made for porphyrin model compounds (*29*) and previous work on sGC (*20*).

RESULTS

Histidine to Alanine Mutants. Site-directed mutagenesis was used to determine which histidine residue serves as the proximal ligand in sGC. All of the conserved histidines in sGC β1(1−385) were individually mutated to alanine. The β1(1−385) mutants were expressed in *E. coli* and purified using methods described previously in addition to the methods described here. Based on the amino acid sequence alignment of the nine known sGC subunits from human, bovine, rat, and *Drosophila*, there are four conserved histidines in the region corresponding to β1(1−385): H105, H134, H220, and H346 (*30, 31*), where the amino acid residue numbers refer to the rat lung sGC β1 sequence. Table 1 summarizes the effects of the histidine to alanine mutations in β1(1−385) on heme binding, electronic absorption spectra, and dimerization. All the histidine to alanine mutants except H105A in β1(1−385) were able to bind heme. Both H220A and H346A contained a stoichiometric equivalent of heme; however, the electronic absorption spectra (Figure 1) showed a Soret peak at 426 nm with a shoulder at 431 nm. This is different from wt β1(1−385) which has a sharp Soret band maximum at 431 nm and a single α/β band (*19*). Addition of CO to either H220A or H346A resulted in formation of a heme−CO complex with a Soret maximum at 423 nm (Table 1). Formation of this complex in the absence of reducing agents indicates that the heme in both these mutants as isolated was ferrous. Furthermore, the spectra of these mutants before addition of CO suggested a mixture of low-spin ferrous (426 nm) and some high-spin ferrous (431 nm) heme. As with wt β1(1−385), H220A and H346A also formed a 5-coordinate nitrosyl complex with NO which has a Soret maximum at 399 nm (Table 1). The presence of a shoulder at 485 nm (not shown) also indicated that the nitrosyl complex is 5-coordinate (*32*). H134A was able to bind heme with a Soret maximum at 431 nm, although this mutant was not purified to homogeneity because of a lower level of expression compared to the other mutants. We were unable to detect any heme bound to the H105A mutant. As described previously (*19*), wt β1(1−385) is a homodimer. Point mutations of H105A or H220A did not affect dimerization; however, H346A was observed to be exclusively monomeric (Table 1).

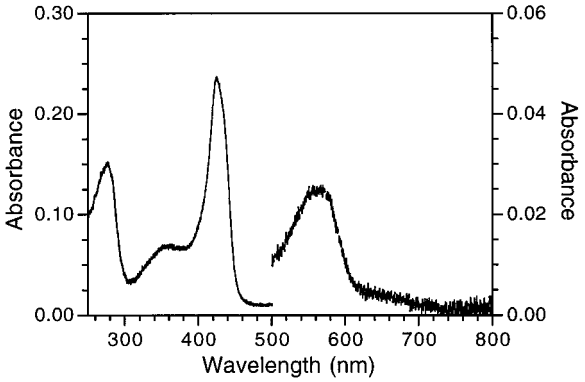

FIGURE 1: Electronic absorption spectrum of the sGC β1(1−385) H220A mutant (2 μM) in 50 mM Hepes, pH 7.4, 150 mM NaCl, 5 mM DTT. The left scale refers to the Soret and protein peak region, and the right scale refers to the α/β region.

Rescue of Heme Binding to H105G. When the H105G mutant was expressed in *E. coli* and purified using the same method used for wt β1(1−385) purification, no heme was detected. However, upon addition of 10 mM imidazole to the growth medium and the purification buffers, H105G(Im) was found to contain a stoichiometric equivalent of heme.

The electronic absorption spectrum of H105G(Im) in the presence of 10 mM imidazole is shown in Figure 2. It had a very sharp Soret peak with a maximum at 423 nm, a shoulder at around 400 nm, and a split α/β band. It also had a δ band with a maximum at 344 nm. The UV−visible spectrum of H105G(Im) in the presence of 10 mM imidazole was different from wt β1(1−385) which contains a 5-coordinate high-spin ferrous heme with a Soret maximum at 431 nm and a single α/β band (*19*). Addition of CO to H105G(Im) did not change the electronic absorption spectrum (data not shown). H105G(Im) did, however, form a cyanide complex which had a distinct electronic absorption spectrum (Figure 3) and which suggested that H105G(Im) contained ferric heme. Resonance Raman spectra of H105G(Im) also indicated that the heme in H105G(Im) as isolated was ferric (see below). The electronic absorption spectrum of H105G(Im) (Figure 2) suggested that the heme in H105G(Im) was a mixture of high-spin 5-coordinate and low-spin 6-coordinate complexes. We tentatively assigned the Soret peak at

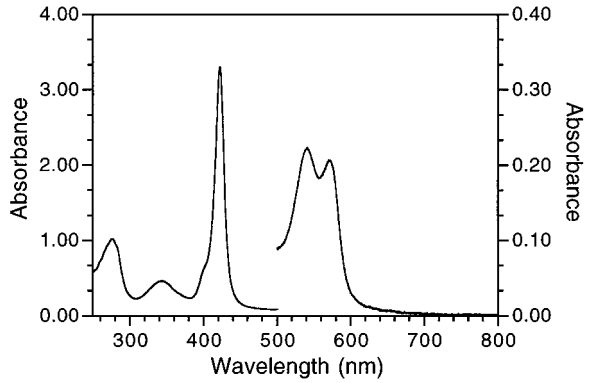

FIGURE 2: Electronic absorption spectrum of sGC β1(1−385) H105G(Im). The sample (20 μM) was isolated in the presence of 10 mM imidazole in 50 mM Hepes, 150 mM NaCl. The left scale refers to the Soret peak and protein peak region, and the right scale refers to the α/β region.

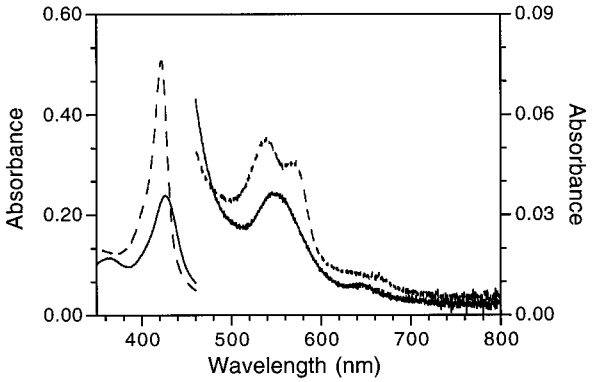

FIGURE 3: Electronic absorption spectrum of the sGC β1(1−385) cyano-complex H105G(Im) (7 μM) in 50 mM Hepes, pH 7.4, 150 mM NaCl, 10 mM imidazole: cyano complex (+250 mM KCN) (—); as isolated (- - -). The left scale refers to the Soret region, and the right scale refers to the α/β region.

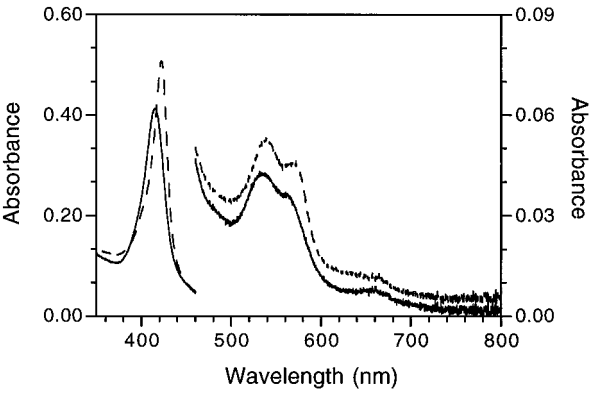

FIGURE 4: Electronic absorption spectrum of the bis(imidazole) complex of sGC β1(1−385) H105G(Im) (7 μM) in 50 mM Hepes, pH 7.4, 150 mM NaCl: bis(imidazole) complex (+300 mM imidazole) (—); as isolated (- - -). The left scale refers to the Soret region, and the right scale refers to the α/β region.

423 nm as that resulting from the 6-coordinate low-spin complex. The sixth ligand may be water, imidazole, or another protein-donated ligand. The shoulder at 400 nm may result from the high-spin, 5-coordinate heme. Addition of more imidazole led to the formation of a bis(imidazole)−heme complex that shifted the Soret maximum from 423 to 415 nm (Figure 4), suggesting that the sixth ligand in H105G-(Im) as isolated was not imidazole. NO reduced the ferric

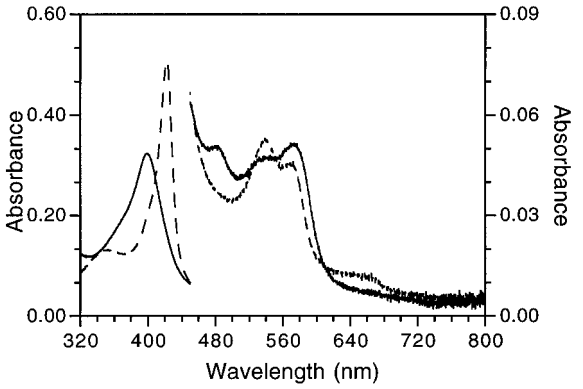

FIGURE 5: Electronic absorption spectrum of the nitrosyl complex of β1(1−385) H105G(Im) (7 μM) in 50 mM Hepes, pH 7.4, 150 mM NaCl, 10 mM imidazole: nitrosyl complex (—); as isolated (- - -). The left scale refers to the Soret region, and the right scale refers to the α/β region.

heme in H105G(Im), and the resulting ferrous heme was able to form a nitrosyl complex with additional NO (Figure 5). The nitrosyl complex of H105G(Im) was identical to that of wt β1(1−385), which is 5-coordinate with a Soret maximum at 399 nm.

Resonance Raman Spectroscopy of H105G(Im). The resonance Raman spectra of wt β1(1−385) and H105G(Im) in the presence of 1 mM imidazole are shown in Figure 6A and B, respectively. The resonance Raman spectrum of the wt β1(1−385) was essentially identical to that of the heterodimeric sGC isolated from bovine lung (*20*). This result further supports our conclusion that the heme environment in wt β1(1−385) is very similar, if not identical, to that of heterodimeric sGC (*19*).

In the high-frequency spectrum of H105G(Im) taken in the presence of 1 mM imidazole (Figure 6A, spectrum b), there was an intense peak at 1374 cm^{-1}(ν_4) which is sensitive to the coordination number and oxidation state of the heme (*33*). The frequency of the ν_4 vibration indicated that the heme in H105G(Im) was most likely ferric, but a 6-coordinate ferrous heme cannot be ruled out. However, based on the observation of a low-intensity ν_3 vibrational mode around 1500 cm^{-1}, we conclude that the heme in H105G(Im) was ferric. This conclusion is consistent with our electronic absorption spectroscopic observations. Upon closer inspection, the ν_3 mode appeared to consist of two vibrations: one at 1501 cm^{-1} and one at 1494 cm^{-1}. The broad band centered at 1627 cm^{-1} in the high-frequency region consists of the ν_{10} and vinyl stretching vibration, ν_{CC}, of both forms of the ferric heme, i.e., 5-coordinate, high-spin and 6-coordinate, low-spin. We expected the ν_{CC} vibration around 1627 cm^{-1}, since this vibration is rather insensitive to the state of the heme (*29*). The shoulder on the higher frequency side can be assigned to the ν_{10} vibration, which is expected around 1630 and 1640 cm^{-1} for 5-coordinate, high-spin and 6-coordinate, low-spin ferric heme, respectively (*29*). This indicated that the heme in H105G(Im) was a mixture of 6-coordinate, low-spin (ν_3 =1501 cm^{-1}) and 5-coordinate, high-spin (ν_3 = 1494 cm^{-1}). In both cases, the ν_4 vibration is expected to be around 1374 cm^{-1}. Finally, no vibrational modes were detected below 275 cm^{-1} for H105G(Im) (Figure 6B, spectrum b).

The reduction of H105G(Im) with dithionite in the presence of imidazole converted the heme to a 5-coordinate,

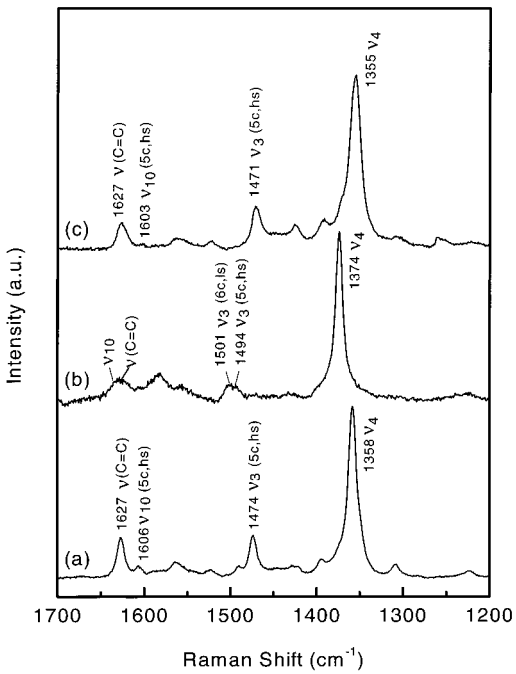

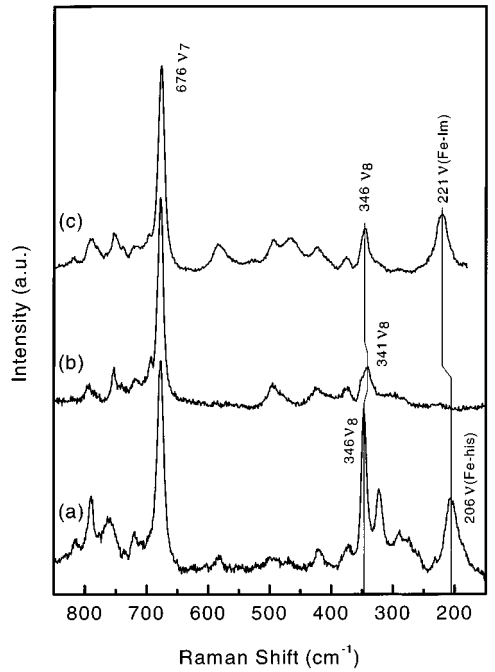

FIGURE 6: High- (A) and low- (B) frequency resonance Raman spectra of the wt β1(1−385) (a) in 50 mM Hepes, pH 7.4, 150 mM NaCl, 5 mM DTT, and the H105G(Im) mutant as isolated (b) and reduced with dithionite (c). The high- and low-frequency spectra are normalized to the ν_4 and 676 cm^{-1} vibrations, respectively. The spectra were collected with 413 nm excitation for the H105G mutant and with 431 nm excitation for wt β1(1−385). The following abbreviations are used in the figure: ν(C═C), vinyl stretching vibration; 5c, 5-coordinate complex; 6c, 6-coordinate complex; hs, high-spin; ls, low-spin. The other ν labels are according to Abe et al. (*28*). The accumulation times for the high-frequency and the low-frequency spectra were 10 min and 30 min, respectively.

high-spin ferrous complex. In the high-frequency resonance Raman spectrum (Figure 6A, spectrum c), this was indicated by the ν_4 vibration at 1355 cm^{-1}, the ν_3 vibration at 1471 cm^{-1}, and the ν_{10} vibration around 1603 cm^{-1}. The most pronounced change, however, was observed in the low-frequency region (Figure 6B, spectrum c), where an intense

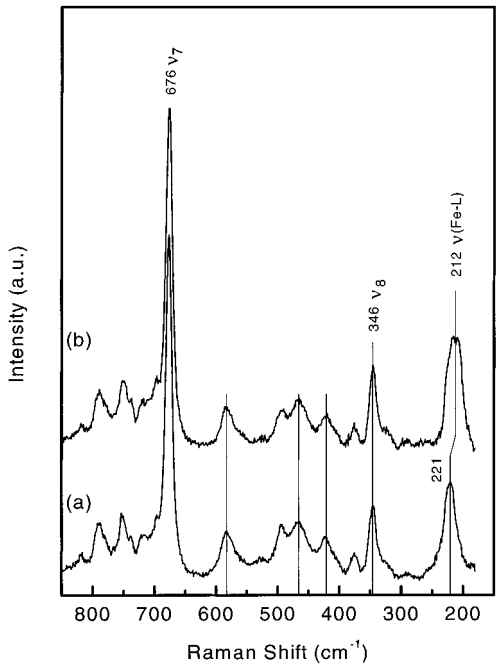

FIGURE 7: Low-frequency resonance spectra of H105G(Im) mutant with 1 mM imidazole (a) and *N*-methylimidazole (b). The spectra were normalized to the 676 cm^{-1} vibrational mode. The spectra were collected with excitation at 413 nm. The accumulation time was 30 min. L = imidazole in spectrum a, and L is a mixture of predominantly *N*-methylimidazole and some imidazole in spectrum b. The lines are drawn to show that no other vibrations are sensitive to the exchange of the proximal ligand.

Raman band appeared at 221 cm^{-1}. Since the 221 cm^{-1} vibrational mode appeared upon reduction of H105G(Im), we assigned this mode to the Fe−N(Im) vibration of the 5-coordinate, high-spin complex formed by the ferrous heme and imidazole in the heme pocket of H105G(Im).

The differences in the intensities of modes from the wt β1(1−385) and the reduced H105G(Im) are most likely related to differences in the excitation wavelengths. In the case of the wt β1(1−385), we used excitation at 431 nm, while excitation at 413 nm was used for H105G(Im). The use of different excitation wavelengths will affect the intensities of vibrational modes, but does not change their frequencies.

Imidazole Serves as the Proximal Ligand in H105G(Im). To show that the imidazole is directly coordinated to the heme Fe in H105G(Im), we carried out ligand exchange and resonance Raman spectroscopic studies. In the low-frequency spectrum of reduced H105G(Im), there was a band at 221 cm^{-1} that was assigned as the Fe−N(Im) stretching mode (Figures 6B and 7). If the added imidazole was indeed coordinated to the heme in H105G(Im), a different Fe−N stretching frequency was expected to be observed upon exchange with *N*-methylimidazole. *N*-Methylimidazole can lead to a vibration frequency downshift of 8−16 cm^{-1} for the Fe−N(Im) stretching mode (*34*). This prediction was verified in the H25A heme oxygenase mutant as a 12 cm^{-1} downshift was observed in this vibration when imidazole was substituted by *N*-methylimidazole (*35*). As shown in Figure 7, a shift from 221 to 212 cm^{-1} was observed when *N*-methylimidazole was substituted for imidazole in the H105G mutant. This result confirmed our assignment of this vibration, which was observed at 221 cm^{-1} for imidazole

and at 212 cm^{-1} for the *N*-methylimidazole, to the Fe−N(Im/MeIm) stretching vibration.

DISCUSSION

A combination of site-directed mutagenesis, UV−visible, and resonance Raman spectroscopic approaches employed in this study has led to the identification of H105 in the sGC β1 subunit as the heme proximal ligand. We not only were able to generate heme-deficient H105 β1(1−385) mutants by site-directed mutagenesis but also were able to rescue heme binding to the H105G mutant by adding imidazole to the culture media and purification buffers.

We have recently localized the heme binding region in sGC to the N-terminal region of the β1 subunit. The N-terminal fragment of the β1 subunit [residues 1−385, β1-(1−385)] was expressed in *E. coli*, purified, and shown to be sufficient for heme binding. Electronic absorption spectroscopic studies have shown that the heme environment in β1(1−385) is very similar to that in the heterodimeric sGC isolated from bovine lung (*19*). In both cases, the heme is 5-coordinate, ferrous, and high-spin with histidine as the only axial ligand (*12*, *19*). Therefore, we used this fragment to identify the heme proximal ligand in sGC. The first step in identifying the heme proximal ligand in sGC was to individually mutate each of the conserved histidines in the heme binding region β1(1−385). All of the histidine mutants except H105A were shown to have the capacity to bind heme (Table 1), suggesting that H105 is likely to be the heme proximal ligand in sGC. The heme deficiency in the H105A mutant of β1(1−385) is probably due to lack of an appropriate heme ligand. These results are also consistent with those from the Koesling group (*31*), who found that, when H105 and other conserved histidine residues in sGC were mutated to phenylalanine and expressed in a baculovirus/SF9 system as a heterodimeric protein (α1β1), only H105F lost the NO-stimulated sGC activity. They also found that the purified H105F mutant was heme-deficient. One explanation for the heme deficiency of the H105F mutant of heterodimeric sGC is that H105 is the heme proximal ligand and that the heme deficiency in the H105F mutant is due to lack of an appropriate heme ligand or alteration of the heme binding site with the larger residue replacement. However, alternative explanations have not been ruled out. For example, H105 may simply play a structural role, and without H105, the heme binding pocket may not fold correctly. Clearly, the heme binding pocket is subject to rather stringent structural requirements since a C78S mutation in the β1 subunit of sGC has also been found to be heme-deficient with no NO-stimulated activity (*36*). The heme deficiency of the C78S mutant apparently does not result from loss of the proximal ligand, but rather to some other structural changes since all evidence supports a histidine residue as the sole axial ligand.

As mentioned above, the only heme-deficient mutants of β1(1−385) are H105A and H105G. The fact that two smaller β1 fragments of sGC [β1(1−345) and β1(1−206)] still bind heme when expressed in *E. coli* and subsequently isolated further supports H105 as the proximal ligand since the conserved histidine residues H220 and H346 are not included in these smaller fragments (Zhao and Marletta, unpublished data). Replacement of the proximal histidine with small residues such as glycine in hemoproteins can, in theory, generate a cavity on the proximal side of the heme binding pocket. In practice, small molecules such as imidazole have been shown to be able to diffuse into the cavity and rescue heme binding as seen with the myoglobin H93G mutant (*37*), the cytochrome *c* peroxidase H175G mutant (*38*), and the horseradish peroxidase H170A mutant (*39*). In these examples, the proximal ligand, as revealed by X-ray crystallography, is known to be histidine and the substituted imidazole in the corresponding mutants was shown to occupy the same site (*37*, *38*). In our case, when imidazole was added to the culture media and purification buffers, H105G(Im) was isolated and found to contain a stoichoimetric equivalent of heme (Figure 2). No heme reconstitution was necessary. One explanation of these results is that imidazole diffuses into the heme binding pocket and then serves as the proximal heme ligand in H105G(Im). However, alternative explanations could not be ruled out, such as the rescue of the structural elements destroyed by the mutation.

To show that the imidazole in H105G(Im) functions as the heme ligand, we carried out ligand exchange experiments and used resonance Raman spectroscopy to detect changes in the heme environment. DePillis et al. demonstrated that the axial imidazole ligand in the H93G myoglobin mutant could be exchanged with other ligands such as *N*-methylimidazole by simply adding an excess of another potential ligand (*40*). To exchange the ligand, H105G(Im) was purified without adding imidazole to the buffer for the last step of the purification (gel filtration). Since this step could be completed in less than 2 h, we were able to isolate H105G-(Im) where more than 80% of the protein still had heme bound. By omitting imidazole in the last purification step, we avoided excess imidazole in the sample which might inhibit the subsequent ligand exchange. We also wanted to avoid a very high concentration of ligand in the exchange process, which could lead to a 6-coordinate complex with H105G(Im). Indeed, when the imidazole concentration reached 250 mM, a 6-coordinate bis(imidazole) complex was formed as revealed by electronic absorption spectroscopy (Figure 4) and resonance Raman spectroscopy (data not shown). Ligand exchange in H105G(Im) was achieved by simply adding the desired ligand directly to the sample at a final concentration of 1 mM. Ferrous H105G(Im) in the presence of 1 mM imidazole was 5-coordinate and high-spin as indicated by the ν_3 at 1471 cm^{-1} and the ν_4 at 1355 cm^{-1} (Figure 6A, spectrum c). In ferrous heme complexes, the Fe−His stretching frequency is usually between 230 and 200 cm^{-1}. We assigned a vibrational mode at 221 cm^{-1} in the ferrous H105G(Im) low-frequency spectrum as the Fe−N(Im) vibration. When imidazole was exchanged with *N*-methylimidazole, the ferrous H105G(MeIm) was still high-spin 5-coordinate as it had the same high-frequency Raman spectrum as H105G(Im) (data not shown). The only Raman peak that shifted in the low-frequency spectrum was the putative Fe−N(Im) vibrational mode, which shifted from 221 to 212 cm^{-1} after ligand exchange. This result indicated that the mode at 221 cm^{-1} is indeed the Fe−N(Im) stretching mode and that imidazole serves as an axial ligand. The large Fe−N vibrational frequency difference between imidazole and *N*-methylimidazole results from mass effects (*35*) and may also reflect a weaker Fe−N bond when *N*-methylimi-

dazole is the ligand. It is possible that this shift results from a structural rescue; however, if that was the case, it is unlikely that this would be the only Raman band to shift. Therefore, from the results of site-directed mutagenesis, electronic absorption, and resonance Raman spectroscopy, we conclude that the H105 in the β1 subunit of sGC is the proximal heme ligand.

We previously reported that the heme environment of wt β1(1−385) is very similar to that of heterodimeric sGC as indicted by electronic absorption spectroscopic studies. Here, resonance Raman spectroscopic studies of wt β1(1−385) further support that conclusion. Both high- and low-frequency resonance Raman spectra of wt β1(1−385) were very similar to those of heterodimeric sGC. The only significant differences observed were the Fe−N(His) stretching vibration and the ν_3 vibration, which is sensitive to both spin and oxidation states of the heme. The Fe−N(His) vibration has a frequency of 204 cm^{-1} in heterodimeric sGC and is observed at 206 cm^{-1} in the wt β1(1−385). The ν_3 vibration is at 1474 cm^{-1} in the wt β1(1−385) (Figure 6A), while it is observed at 1471 cm^{-1} in the heterodimeric sGC (*20*). These differences are likely to be due to the effects of minor changes in the heme binding pocket of the wt β1(1−385) with respect to the heterodimeric sGC.

The ferrous heme in reduced H105G(Im) is 5-coordinate, high-spin as indicated by the resonance Raman spectra. Remarkably, the high- and low-frequency spectra of the reduced H105G(Im) in the presence of imidazole and those of wt β1(1−385) are almost identical. Three vibrations are different: the Fe−N(Im/His), the ν_3 vibration, and the ν_4 vibration. The ν_3 vibration has the same frequency as in the heterodimeric sGC, but is 3 cm^{-1} lower than that in wt β1(1−385). The ν_4 vibration is 3 cm^{-1} lower than that in both the wt β1(1−385) and the heterodimeric sGC. The putative Fe−N(Im) stretching frequency of H105G(Im) is much higher than that of the wt β1(1−385) (221 vs 206 cm^{-1}). This shift indicates that the Fe−N(Im) bond in H105G is stronger than the Fe−N(His) in wt β1(1−385) and heterodimeric sGC. The lack of a covalent bond between the imidazole and the protein could account for this difference.

It is interesting that the heme in H105G(Im) as isolated is ferric, while that in heterodimeric sGC and wt β1(1−385) is ferrous (*12*, *19*). Like the ferrous heme in heterodimeric sGC and β1(1−385), the ferrous heme in H105G(Im) (after dithionite reduction) is also 5-coordinate, high-spin, as indicated by resonance Raman spectroscopy (Figure 6A and B). Neither heterodimeric sGC (*12*) nor wt β1(1−385) (*19*) binds oxygen. The low affinity of sGC and wt β1(1−385) for oxygen may be due, in part, to the weak Fe−His bond detected by resonance Raman spectra [Figure 6B, spectrum a and (*20*)]. In model studies, it has been shown that a stronger His−Fe bond leads to a stronger Fe−O bond (*41*). In H105G(Im), the Fe−Im stretching vibration is at 221 cm^{-1} [sGC, 204 cm^{-1}; β1(1−385), 206 cm^{-1}], indicating a stronger Fe−N bond. The stronger Fe−Im bond may lead to an increase in O_2 affinity for H105G(Im). If O_2 binds to ferrous heme in H105G(Im), it may oxidize the heme, resulting in the isolation of ferric H105G(Im). Indeed, when the ferrous heme of H105G(Im) was exposed to air, it was converted to ferric heme instantly (Zhao, Schelvis, Babcock, and Marletta, unpublished data). It has also been reported that the proximal ligand can affect the redox potential of heme (*42*). When more negative charge exists in the imidazole ring, the His−Fe bond becomes stronger and also leads to a decrease of the Fe^{3+}/Fe^{2+} reduction potential, which stabilizes the Fe^{3+} form relative to the Fe^{2+} oxidation state (*42*). Therefore, a stronger Fe−Im bond may partially explain why H105G(Im) is ferric while sGC and wt β1(1−385) are ferrous.

The molecular mechanisms involved in NO activation as well as the mechanism of deactivation of sGC remain as critical unanswered questions that must be answered in order to understand the biochemical basis of NO action. Our results that identify H105 as the proximal heme ligand in the β1 subunit of sGC provide the basis for further study of these important questions.

ACKNOWLEDGMENT

We thank Jason M. Perry for helpful discussions, Amy R. Hurshman and Kristin M. Rusche for advice and help with handling CO and NO, and the Marletta group for critical comments on the manuscript.

REFERENCES

1. Garbers, D. L., & Lowe, D. G. (1994) *J. Biol. Chem. 269*, 30741−30744.
2. Yuen, P. S. T., & Garbers, D. L. (1992) *Annu. Rev. Neurosci. 15*, 193−225.
3. Wong, S. K.-F., & Garbers, D. L. (1992) *J. Clin. Invest. 90*, 299−305.
4. Arnold, W. P., Mittal, C. K., Katsuki, S., & Murad, F. (1977) *Proc. Natl. Acad. Sci. U.S.A. 74*, 3203−3207.
5. Marletta, M. A. (1994) *Cell 78*, 927−930.
6. Bredt, D. S., & Snyder, S. H. (1994) *Annu. Rev. Biochem. 63*, 175−195.
7. Moncada, S., Palmer, R. M. J., & Higgs, E. A. (1991) *Pharmacol. Rev. 43*, 109−142.
8. Garbers, D. L. (1979) *J. Biol. Chem. 254*, 240−243.
9. Gerzer, R., Böhme, E., Hofmann, F., & Schultz, G. (1981) *FEBS Lett. 132*, 71−74.
10. Kamisaki, Y., Saheki, S., Nakane, M., Palmieri, J. A., Kuno, T., Chang, B. Y., Waldman, S. A., & Murad, F. (1986) *J. Biol. Chem. 261*, 7236−7241.
11. Mulsch, A., & Gerzer, R. (1991) *Methods Enzymol. 195*, 377−383.
12. Stone, J. R., & Marletta, M. A. (1994) *Biochemistry 33*, 5636−5640.
13. Yuen, P. S. T., Potter, L. R., & Garbers, D. L. (1990) *Biochemistry 29*, 10872−10878.
14. Harteneck, C., Wedel, B., Koesling, D., Malkewitz, J., Bohme, E., & Schultz, G. (1991) *FEBS Lett. 292*, 217−222.
15. Harteneck, C., Koesling, D., Soling, A., Schultz, G., & Bohme, E. (1990) *FEBS Lett. 272*, 221−223.
16. Buechler, W. A., Nakane, M., & Murad, F. (1991) *Biochem. Biophys. Res. Commun. 174*, 351−357.
17. Foerster, J., Harteneck, C., Malkewitz, J., Schultz, G., & Koesling, D. (1996) *Eur. J. Biochem. 240*, 380−386.
18. Wedel, B., Harteneck, C., Foerster, J., Friebe, A., Schultz, G., & Koesling, D. (1995) *J. Biol. Chem. 270*, 24871−24875.
19. Zhao, Y., & Marletta, M. A. (1997) *Biochemistry 36*, 15959−15964.
20. Deinum, G., Stone, J. R., Babcock, G. T., & Marletta, M. A. (1996) *Biochemistry 35*, 1540−1547.
21. Kim, S., Deinum, G., Gardner, M. T., Marletta, M. A., & Babcock, G. T. (1996) *J. Am. Chem. Soc. 118*, 8769−8770.
22. Stone, J. R., Sands, R. H., Dunham, W. R., & Marletta, M. A. (1995) *Biochem. Biophys. Res. Commun. 207*, 572−577.
23. Dierks, E. A., Hu, S., Vogel, K. M., Yu, A. E., Spiro, T. G., & Burstyn, J. N. (1997) *J. Am. Chem. Soc. 119*.
24. Decatur, S. M., DePillis, G. D., & Boxer, S. G. (1996) *Biochemistry 35*, 3925−3932.

25. Yu, A. E., Hu, S., Spiro, T. G., & Burstyn, J. N. (1994) *J. Am. Chem. Soc. 116*, 4117−4118.
26. Ho, S. N., Hunt, H. D., Horton, R. M., Pullen, J. K., & Pease, L. R. (1989) *Gene 77*, 51−59.
27. White, K. A., & Marletta, M. A. (1992) *Biochemistry 31*, 6627−6631.
28. Abe, M., Kitagawa, T., & Kyogoku, Y. (1978) *J. Chem. Phys. 69*, 4526−4534.
29. Choi, S., Lee, J. J., Wei, Y. H., & Spiro, T. G. (1983) *J. Am. Chem. Soc. 105*, 3692−3707.
30. Stone, J. R., & Marletta, M. A. (1995) *Biochemistry 34*, 14668−14674.
31. Wedel, B., Humbert, P., Harteneck, C., Foerster, J., Malkewitz, J., Bohme, E., Schultz, G., & Koesling, D. (1994) *Proc. Natl. Acad. Sci. U.S.A. 91*, 2592−2596.
32. Yoshimura, T., Suzuki, S., Nakahara, A., Iwasaki, H., Masuko, M., & Matsubara, T. (1986) *Biochemistry 25*, 2436−2442.
33. Babcock, G. T. (1988) in *Biological Applications of Raman Spectroscopy* (Spiro, T. G., Ed.) pp 293−346, John Wiley & Sons Inc., New York.
34. Wells, A. V., Sage, J. T., Morikis, D., Champion, P. M., Chiu, M. L., & Sligar, S. G. (1991) *J. Am. Chem. Soc. 113*, 9655−9660.
35. Wilks, A., Sun, J., Loehr, T. M., & Ortiz de Montellano, P. R. (1995) *J. Am. Chem. Soc. 117*, 2925−2926.
36. Friebe, A., Wedel, B., Harteneck, C., Foerster, J., Schultz, G., & Koesling, D. (1997) *Biochemistry 36*, 1194−1198.
37. Barrick, D. (1994) *Biochemistry 33*, 6546−6554.
38. McRee, D. E., Jensen, G. M., Fitzgerald, M. M., Siegel, H. A., & Goodin, D. B. (1994) *Proc. Natl. Acad. Sci. U.S.A. 91*, 12847−12851.
39. Newmyer, S. L., Sun, J., Loehr, T. M., & Ortiz de Montellano, P. R. (1996) *Biochemistry 35*, 12788−12795.
40. DePillis, G. D., Decatur, S. M., Barrick, D., & Boxer, S. G. (1994) *J. Am. Chem. Soc. 116*, 6981−6982.
41. Oertling, W. A., Kean, R. T., Wever, R., & Babcock, G. T. (1990) *Inorg. Chem. 29*, 2633−2645.
42. Choudhury, K., Sundaramoorthy, M., Hickman, A., Yonetani, T., Woehl, E., Dunn, M. F., & Poulos, T. L. (1994) *J. Biol. Chem. 269*, 20239−20249.

BI972686M